Research Square

Preprints are preliminary reports that have not undergone peer review.
They should not be considered conclusive, used to inform clinical practice,
or referenced by the media as validated information.

Nanosheet-Based g-C_3N_4/$NiFe_2O_4$ Composite as an Efficient Heterogeneous Catalyst for Synthesis of 14-Aryl-14H-Dibenzo[a,j]xanthenes in Water: Cytotoxic Activity and Molecular Docking Studies

Leila Amiri-Zirtol
shiraz university of medical sciences
Asiyeh Sheikhzadeh Takabi
Shahid Chamran University of Ahvaz
Sara Sadeghian
shiraz university of medical sciences
Zahra Karimi
Amirkabir University of Technology
Seyed Hesamedin Nabavizadeh
shiraz university of medical sciences
Soghra Khabnadideh
khabns@sums.ac.ir

shiraz university of medical sciences

Article

Keywords: Graphitic carbon nitride, Anticancer, Xanthene, Catalyst

Posted Date: October 23rd, 2026

DOI: https://doi.org/10.21203/rs.3.rs-11032785/v1

License: This work is licensed under a Creative Commons Attribution 4.0 International License.
Read Full License

Additional Declarations: No competing interests reported.

Abstract

Here, we present the design and synthesis of a highly efficient catalyst based on mesoporous nanosheet graphitic carbon nitride (g-C_3N_4) functionalized with magnetic $NiFe_2O_4$ nanoparticles. This composite has been employed, for the first time, as a heterogenic catalyst in multi-component reactions (MCRs) demonstrating remarkable catalytic activity and reusability. The synthesized composite (g-C_3N_4/$NiFe_2O_4$) was thoroughly characterized using FT-IR, FE-SEM, EDX, mapping, XRD, VSM, and TGA. The catalytic activity of the composite was investigated in the synthesis of some xanthene derivatives **(3a-3g)** under green and mild reaction conditions using H_2O as green solvent at reflux temperature which led to excellent yields in remarkably short reaction times. Notably, the catalyst exhibited high stability and reusability, maintaining its efficiency over six consecutive cycles without significant activity losses. Furthermore, the cytotoxicity properties of the synthesized xanthene compounds were evaluated against MCF-7 cancerous cell line. Among the tested molecules, compounds **3e** and **3f** exhibited the highest cytotoxic activity within the series, with IC_{50} values of 50.0 ± 2.26 µM and 89.6 ± 5.30 µM, respectively. Furthermore, molecular docking study was performed to investigate the interaction mode of this class of compounds with Estrogen Receptor alpha (ERα), which is overexpress in MCF-7 cell line. The results showed favorable interaction of the active compounds with this receptor.

1. Introduction

The development of simple and cost-effective protocols for preparing important heterocyclic compounds has become a crucial focus (1–4). Designing efficient catalyst recycling systems has become a critical area of focus due to its significant economic and environmental benefits (5, 6). Solid catalysts have emerged as highly effective alternatives to homogeneous catalysts, gaining significant attention due to their low toxicity, ease of separation, improved reusability, corrosion resistance and alignment with green chemistry principles (7–9). These catalysts, with high efficiency, good stability, and recyclability, have emerged as one of the fundamental challenges in modern chemistry and green processes design. In this context, the incorporation of metallic magnetic nanoparticles such as Fe_3O_4, $CoFe_2O_4$, and $NiFe_2O_4$ into catalyst structures has attracted considerable attention. In addition to being acidic, they have other distinctive features, including high specific surface area, excellent thermal and chemical stability, and strong magnetic behavior. On the other hand, these nanoparticles enable convenient catalyst recovery without the need for filtration or centrifugation. However, challenges such as particle aggregation, reduction of active surface area, and consequent drop-in catalytic activity have prevented these materials from providing ideal performance on their own (10–12).

Recent researches have concentrated on using of strong and electrically conductive non-metallic supports, like graphene oxide, silica, and carbon nanotubes, for the immobilization of nanoparticles in order to get around these problems. Because of its nitrogen-rich tri-s-triazine structure, which permits robust interactions with metal ions, g-C_3N_4 holds a special place among these supports. Nanosheet graphitic carbon nitride (g-C_3N_4), a semiconductor material with a layered structure, has drawn a lot of

interest because of its excellent thermal stability, low cost, biocompatibility, and nitrogen-based active sites. Maintaining or enhancing the activities of recyclable catalytic systems, particularly those using solid reagents and catalysts, compared to their homogeneous counterparts, possess several challenges (13–15). This type of catalysts offers a promising approach to enhancing the sustainability and efficiency of acid-catalyzed reactions in both academic and industrial settings (16, 17).

On the other hands, Multi Component Reactions (MCRs) achieve high atom economy by incorporating most reactant atoms into the final product, minimizing by-products. This contrasts with traditional linear synthesis, which generates intermediate wastes at each purification step. The convergent nature of MCRs reduces solvent and auxiliary chemical use by up to 50% compared to stepwise approaches (18–21).

Xanthene derivatives are a notable class of oxygen-containing heterocyclic compounds that have garnered significant attention due to their diverse and valuable biological and pharmaceutical properties. These compounds consist of an oxygen-containing central heterocyclic structure with two additional cyclic structures fused to it, which contributes to their unique properties and applications (22, 23). The diverse biological activities and pharmaceutical potential of xanthene derivatives make them an attractive area of research in both academia and industry (24). The synthesis of xanthene's has been explored using a wide variety of catalysts, reflecting the ongoing interest in optimizing reaction conditions and improving efficiency (25). These catalysts include: Natural Acidic Ionic Liquid Immobilized on Magnetic Silica (26), Task-Specific Di cationic Acidic IL (27), Amberlyst-15 (28), p-Toluene sulfonic Acid (p-TSA) (29), Iron (III) Hydrogen Sulfate ($Fe(HSO_4)_3$) (30), Boron Trifluoride on Silica ($BF_3{\cdot}SiO_2$) (31), Dipyridine Cobalt Chloride (32), Sulfamic acid@MCM-41 (33). However, these methods often come with disadvantages such as harsh reaction conditions, lengthy reaction times, the need for specialized equipment, and the use of hazardous solvents. Therefore, developing alternative methods to synthesize xanthene derivatives without relying on toxic catalysts and hazardous solvents is indeed a crucial goal for several reasons: environmental impact, health and safety, sustainability, regulatory compliance, and cost efficiency (34, 35).

Here, we reported the preparation and characterization of $NiFe_2O_4$-modified g-C_3N_4 as a heterogeneous catalyst. The $gC_3N_4/NiFe_2O_4$ magnetic composite has attracted significant attention due to its versatile physicochemical properties and its amphoteric nature, leading to various applications (36, 37). Recent studies have highlighted the versatility of $NiFe_2O_4$/g-C_3N_4 composites in various catalytic applications. For instance, Maleki et al. developed a magnetic $NiFe_2O_4$/g-C_3N_4 catalyst for biodiesel production assisted by ultrasonic irradiation (38). In another study, $NiFe_2O_4$/g-C_3N_4 was utilized as a heterogeneous magnetic photocatalyst, demonstrating enhanced performance for dye degradation under visible-light irradiation (39). Most recently, have highlighted its efficacy in environmental applications, such as the activation of peroxymonosulfate for the degradation of antibiotics (40, 41).

Specifically, the $NiFe_2O_4$ component provides Lewis acidic sites through its positive metal ions (Ni^{+2} and Fe^{+3}). Concurrently, the g-C_3N_4 framework contributes not only through its nitrogen-rich basic sites but also by providing an electron-rich environment that facilitates the adsorption and activation of reactants via enhanced electron transfer (38, 41). However, despite these divers applications, the utilization of this specific composite for the efficient synthesis of xanthene derivatives through multi-component reactions remains unexplored. To the best of our knowledge, this study represents the first application of $NiFe_2O_4$/g-C_3N_4 as a magnetically recoverable heterogeneous catalyst for the one-pot multicomponent synthesis of 14-Aryl-14H-Dibenzo[a,j]xanthene derivative. The reaction was carried out under specific conditions, including H_2O as green solvent. We characterized the structure of the synthesized g-C_3N_4/$NiFe_2O_4$ composite using various analytical techniques, including FT-IR, FE-SEM, EDX, XRD, VSM, and TGA. Then the catalyst's activity was evaluated in the one-pot synthesis of some xanthene derivatives and several xanthene analogues **(3a-3g)** were prepared using this catalyst under suitable conditions. Additionally, cytotoxic activity of the synthesized compounds, was investigated on MCF-7 cancerous cell line in comparison to erlotinib as positive control. Molecular docking study was also performed to investigate the interaction modes of this class of compounds with Estrogen Receptor alpha (ERα), which is overexpressed in the MCF-7 cell line.

2. Results and discussion

In this research g-C_3N_4 was created and manufactured as a catalyst according to previously described technique (42). The g-C_3N_4/$NiFe_2O_4$ composite exhibited high catalytic efficiency, owing to its dual-functional acid-base properties. Specifically, the Ni^{+2} and Fe^{+3} in $NiFe_2O_4$ act as Lewis acid sites, whereas the g-C_3N_4 component provides basic nitrogen sites and an electron-rich platform that promotes reactant activation via improved electron transfer (38, 41). This dual-functional synergy is instrumental in driving the synthesis of 14-Aryl-14H-Dibenzo[a,j]xanthenes. The second stage involved exposing of these nanolayers to $NiFe_2O_4$, which covalently bonded to their surface and surrounding environment. Formation of covalent bond between $NiFe_2O_4$ and g-C_3N_4 enhances the stability of the catalyst. Additionally, using g-C_3N_4 as a support provides a large surface area, facilitating the dispersion of the acidic sites generated by the ring opening of $NiFe_2O_4$ over a wide surface. This dispersion enables the efficient utilization of an appropriate amount of $NiFe_2O_4$ in the reaction. A variety of analytical methods were used to characterize the produced nanocomposite, including FT-IR, FE-SEM, EDX, mapping and XRD. The newly synthesized catalyst showed outstanding performance and good stability in the synthesis of xanthene derivatives.

2.1. Catalyst identification

2.1.1. FT-IR analysis

The FT-IR spectrum of the synthesized nanocatalyst is presented in Fig. 1. Comparison of this spectrum with the FT-IR spectrum of nano- g-C_3N_4/$NiFe_2O_4$, along with the observed spectral changes and the emergence of new peaks, confirms the successful modification of g-C_3N_4 by $NiFe_2O_4$. The peak observed at 3196 cm^{-1} corresponds to NH and OH groups. The peaks observed at 2925 cm^{-1} and 2895 cm^{-1} correspond to CH stretching vibrations of alkane chains, confirming the presence of these functional groups in the synthesized nanocatalyst. The peak at 600 cm^{-1} corresponds to the Fe-O groups. These features provide strong evidence of the $NiFe_2O_4$ structure in our nanocatalyst. The characteristic peaks observed in the FT-IR pattern confirm the formation of g-C_3N_4/$NiFe_2O_4$ which is in good agreement with previous studies (41, 43).

2.1.2. EDX analysis

Energy-dispersive X-ray (EDX) analysis was carried out to confirm the presence of $NiFe_2O_4$ in the nano-g-C_3N_4/$NiFe_2O_4$ composite. As shown in Fig. 2, the EDX spectrum clearly indicates the presence of C, N, O, Ni, and Fe elements, with their respective weight percentages of 21.06, 35.3, 31.11, 3.66 and 8.5, confirming the successful incorporation of $NiFe_2O_4$ onto the g-C_3N_4 surface.

2.1.3. FE-SEM analysis

The morphology of the synthesized nanocatalyst was examined using SEM analysis (Fig. 3). Scanning electron microscopy (SEM) reveal that the nano- g-C_3N_4/$NiFe_2O_4$ composite contains densely grafted $NiFe_2O_4$ nanoparticles uniformly distributed across the g-C_3N_4 sheets, confirming the successful decoration of the g-C_3N_4 framework with $NiFe_2O_4$.This morphological observation is consistent with previously reported studies (44, 45).

2.1.4. X-ray Diffraction (XRD) Analysis

Figure 4 presents the X-ray diffraction (XRD) patterns provided for g-C_3N_4 (blue) and g-C_3N_4/$NiFe_2O_4$ (red) confirm the successful synthesis and combination of these materials. The distinct diffraction peaks correspond well with expected crystallographic features of each phase (JCPDS card no 00-044-1485 for $NiFe_2O_4$ and JCPDS card no 00-012-0212 for g-C_3N_4) (46). The g-C_3N_4 sample displays two main peaks at 2θ ~ 13 and 27.5 and small peaks at higher 2θ. The peak at 13° is typically assigned to the (100) plane, representing the in-plane repeating structural motif of tri-s-triazine units. The dominant peak at 27.5° is associated with the (002) plane, reflecting the interlayer stacking of conjugated aromatic systems within g-C_3N_4 (45, 47).

Upon forming the composite, all the original g-C_3N_4 peaks remain visible, indicating the preservation of its layered structure. New and sharp peaks appear throughout the scan in the red pattern, matching well with standard spinel $NiFe_2O_4$, which confirms its successful loading on the g-C_3N_4 matrix. The intensities and multiplicity of $NiFe_2O_4$ peaks in the composite suggest a high degree of crystallinity and good

dispersion on the g-C_3N_4 support. The coexistence of all g-C_3N_4 peaks with additional $NiFe_2O_4$ peaks in the composite sample proves successful heterojunction formation. No significant shift or disappearance of main peaks suggests that there is interfacial contact but no significant destruction of the original layered or spinel crystal phases. Such nanocomposites are attractive for applications such as photocatalysis and magnetically-separable catalysts due to synergistic effects from the combined phases (14, 48).

2.1.5. VSM analysis

The magnetic properties of the g-C_3N_4/$NiFe_2O_4$ catalyst were investigated using a vibrating sample magnetometer (VSM) at room temperature (Fig. 5). As shown in Fig. 5, the catalyst exhibits clear magnetic behavior with a saturation magnetization value of approximately 7.5 emu g^{-1} under an applied magnetic field of 9800 Oe. These results confirm the successful synthesis of a magnetic inorganocatalyst that can be conveniently separated from the reaction medium using an external magnet.

The magnetic behavior of the g-C_3N_4/$NiFe_2O_4$ composite enables convenient catalyst recovery from the reaction mixture using an external magnet. As shown in Fig. 6, when a magnet is placed near the reaction vessel, the catalyst particles are rapidly attracted and collected on the wall of the beaker. The separation process is completed within approximately 10 second, indicating a sufficiently strong magnetic response for fast and practical catalyst recovery.

2.1.6. TGA analysis

The TGA curve of g-C_3N_4/$NiFe_2O_4$ was showed in Fig. 7. The TGA profile reveals a multi-stage thermal degradation process. The first stage, occurring near 100°C, is associated with the evaporation of moisture. Subsequently, the composite exhibits a gradual weight reduction until reaching a critical degradation temperature of 510°C. Beyond this point, a rapid and significant weight loss is observed, reaching approximately 60% by 600°C, which is attributed to the structural decomposition of the g-C_3N_4 framework and the associated nanoparticles. The remaining 20% residue at 600°C corresponds to the stable inorganic components of the composite. Consequently, the thermal analysis confirms that the synthesized catalyst maintains its structural integrity up to 510°C, demonstrating its suitability for thermally demanding catalytic processes.

2.2. Optimization of the reaction conditions for synthesis of xanthene derivatives

A model reaction for the synthesis of **3d** was selected and tested under different conditions to optimize the process. Initially, the reaction was performed with g-C_3N_4, $NiFe_2O_4$ and g-C_3N_4/$NiFe_2O_4$ as a catalyst, using ethanol as a solvent, at room temperature (Table 1, entries 1–3). The results show high efficacy of our catalyst in progress of the reaction. In the next step, considering the solvent's importance as a key

factor in synthesis, as well as its impact on safety and efficiency, the model reaction was tested in EtOH, H_2O, and solvent-free conditions (Table 1, entries 3–5). The results indicated that the best performance was achieved using EtOH and H_2O. Given that H_2O is a green, readily available solvent, it was selected as the optimal reaction medium. The effect of temperature on the model reaction was also investigated. As shown in Table 1, the best performance was achieved at Reflux (Table 1, entries 5–8). The optimal amount of catalyst required for the model reaction was also determined (Table 1, entries 8–10). The reaction was carried out using 0.04 g of catalyst per 1 mmol of substrate. The findings highlight the suitability of g-C_3N_4/$NiFe_2O_4$ as an effective catalyst for improving reaction yields. Ultimately, the optimal reaction conditions were identified as 0.04 g of catalyst in H_2O at Reflux, yielding the best results (Table 1, entry 9).

Table 1
Optimization of the reaction conditions for synthesis of **3d**[a]

Entry	Catalyst	Weight (g)	Solvent	Temp. (°C)	Time (min)	Yield (%)
1	g-C_3N_4	0.05	Ethanol	r.t.	60	Trace
2	$NiFe_2O_4$	0.05	Ethanol	r.t.	100	70
3	g-C_3N_4/$NiFe_2O_4$	0.05	Ethanol	r.t.	60	80
4	g-C_3N_4/$NiFe_2O_4$	0.05	Solvent free	r.t.	80	75
5	g-C_3N_4/$NiFe_2O_4$	0.05	H_2O	r.t.	60	75
6	g-C_3N4/$NiFe_2O_4$	0.05	H_2O	60	35	90
7	g-C_3N_4/$NiFe_2O_4$	0.05	H_2O	80	15	96
8	g-C_3N_4/$NiFe_2O_4$	0.05	H_2O	Reflux	5	96
9	**g-C_3N_4/$NiFe_2O_4$**	**0.04**	**H_2O**	**Reflux**	**5**	**96**
10	g-C_3N4/$NiFe_2O_4$	0.03	H_2O	Reflux	10	90

[a]Reaction conditions:4-nitrobenzaldehyde (1 mmol), 2-naphthol (2 mmol). All yields are isolated products

2.3. Synthesis of xanthene derivatives

Upon optimizing the reaction conditions, xanthene derivatives were synthesized under the refined parameters, with the results detailed in Table 2. A variety of aromatic aldehydes, encompassing both electron-withdrawing and electron-donating groups, were tested in these reactions. The data revealed that aldehydes containing electron-withdrawing groups, such as NO_2 and Cl, exhibited significantly faster reaction rates and shorter reaction times. In contrast, aldehydes like 4-hydroxybenzaldehyde and 4-methoxybenzaldehyde necessitated longer reaction times to achieve satisfactory yields. The synthesized compounds were characterized by melting point, FT-IR and also NMR spectra for **3a, 3b**, and **3g** (supplementary file).

Table 2
Synthesis of xanthene derivatives **3a-3g**

Entry	Product	Time (min)	Yield (%)[a]	m. p. (℃, found)
3a		15	90	182–185 (49)
3b		5	96	211–214 (50)
3c		5	98	282–283 (49)
3d		5	96	312–316 (50)
3e		15	90	240–243 (51)
3f		15	88	199–203 (51)
3g		10	90	224–226 (50)

[a]All yields are isolated products

The proposed catalytic mechanism for the synthesis of xanthene compounds over the g-C_3N_4/$NiFe_2O_4$ composite is illustrated in Fig. 8. Based on the nature of the catalyst, the reaction is envisioned to initiate *via* the generation of a carbocation intermediate through the interaction of the substrate with the acidic sites. Intermediate I resulted from the nucleophilic attack of the 2-naphthol molecule towards the activated aldehyde center. This is followed by the formation of intermediate II, which subsequently undergo dehydration to yield the final xanthene products. This pathway is consistent with the electrophilic nature of similar metal-oxide-based catalysts reported in the literature (52, 53).

2.4. Hot filtration test

To further validate the recyclability and heterogeneous nature of nano g-C_3N_4/$NiFe_2O_4$, a hot filtration test was conducted on a model reaction. After 2 minutes from the start of the reaction, the catalyst was removed from the reaction mixture via filtration, and the progress of the reaction was systematically monitored. Notably, no further conversion was detected in the filtrate, providing strong evidence for the true heterogeneity of the catalyst and confirming its structural stability and sustained activity under the applied reaction conditions.

2.5. Reusability of the catalyst

A comprehensive investigation was conducted to assess the reusability of nano g-C_3N_4/$NiFe_2O_4$ in a model reaction. Following each reaction cycle, the catalyst was efficiently recovered from the reaction medium, thoroughly washed with ethyl acetate, and dried under a vacuum. After being replenished with fresh starting materials, the regenerated catalyst was directly reutilized in subsequent runs without requiring additional treatment. Remarkably, nano g-C_3N_4/$NiFe_2O_4$ demonstrated excellent stability, maintaining its catalytic activity over 6 consecutive cycles without any significant decline in performance (Fig. 9).

FT-IR spectra were performed after the reaction to evaluate the structural integrity of the catalyst. The striking similarity between the fresh and used catalyst spectra suggests negligible structural degradation, providing strong evidence for the robustness and reusability of nano g-C_3N_4/$NiFe_2O_4$ under the applied reaction conditions (Fig. 10).

2.6. Comparison of the catalyst's performance with literature

Our catalyst’s performance in the model reaction was systematically compared with previously reported methods to assess the catalytic efficiency and effectiveness of the newly developed catalyst in xanthene synthesis (Table 3). The findings demonstrate several distinct advantages of this catalytic system over conventional approaches, including facile recovery and recyclability, high product yield, significantly reduced reaction time, and operating under mild conditions. These attributes collectively highlight the proposed catalyst's superior efficiency, sustainability, and practical applicability, making it a promising alternative for green and efficient organic synthesis.

Table 3
Comparison of the catalytic activity of nano g-C_3N_4/$NiFe_2O_4$ with other catalysts in synthesis of xanthene derivatives

Entry	Catalyst/ Temp / Solvent/Time	Yield (%)	Ref.
1	Fe_3O_4@COF-SO_3H/80^oC/S-F/5 min	96	(54)
2	GO-$CuFe_2O_4$ / 125^oC/ Water / 15 min	92	(55)
3	$CuSO_4.5H_2O$ / 80^oC/ S-F/5(h)	95	(49)
4	$NiCuFe_2O_4$/ UT/Water/ 6 min	98	(53)
5	Phosphosulfonic acid/110^oC/45min	95	(56)
6	Cucurbit[6]uril-OSO3H/110^oC/35min	95	(57)
7	**g-C_3N_4/$NiFe_2O_4$/H_2O/Reflux/5 min**	**96**	**This work**

2.7. Cytotoxicity activity

All the synthesized compounds (**3a-3g**) were screened against the human cancer cell line (MCF-7) to investigate the cytotoxic potential of this class of compounds. The results are summarized in Table 4, with IC_{50} values expressed in μM units. In this assay, erlotinib was selected as positive control. According to the results, several of the tested derivatives exhibited moderate cytotoxic activity against the MCF-7 cell line. Among the evaluated compounds, derivatives **3e** and **3f** showed the highest activity within the series, with IC_{50} values of 50.0 ± 2.26 μM and 89.6 ± 5.30 μM, respectively. The cytotoxic effect of compound **3e** was found to be comparable to that of erlotinib under the experimental conditions employed. Compounds **3a**, **3b**, **3d**, and **3g** exhibited the lowest cytotoxicity against the MCF-7 cell line, with IC_{50} values greater than 200 μM. The findings suggest that substitutions on the phenyl moiety significantly impact the cytotoxic efficacy of this group of compounds. Specifically, the presence of electron-donating groups such as OH and OMe appears to be more favorable than electron-withdrawing groups like Cl and NO_2, as well as alkyl substitutions like methyl.

Table 4
The *in vitro* cytotoxic activity of the synthesized derivatives (**3a-3g**) against MCF-7 cell line

Entry	R	IC_{50} ± SD (μM)
		MCF-7
3a	H	> 200
3b	3-NO_2	> 200
3c	4-Cl	133.7 ± 8.27
3d	4-NO_2	> 200
3e	4-OH	50.0 ± 2.26
3f	4-OMe	89.6 ± 5.30
3g	4-Me	> 200
erlotinib	----	35.5 ± 0.40

2.8. Molecular docking study

Estrogen receptor alpha (ERα) is overexpressed in the MCF-7 cell line (58, 59), therefore, this receptor with the PDB code of 3ERT, was selected for molecular docking studies. The reliability of the molecular docking protocol was validated through a re-docking procedure of the co-crystallized ligand (OHT) into the active site of ERα. The superimposition of the re-docked pose with the crystallographic binding mode yielded a root-mean-square deviation (RMSD) value of less than 2.0 Å, confirming the accuracy and reproducibility of the docking method.

The interactions of compound **3e**, identified as potent compound, and those of **3d** and **3g**, identified as inactive compounds, along with erlotinib as the reference drug, are represented in Fig. 11. Compound **3e**, with binding affinity of -10.3 kcal/mol, showed effective interactions with specific amino acids in the active site of receptor, including Asp351, Trp383, and Val534. Compound **3e** formed a hydrogen bond with Val534, as well as a π-anion interaction with Asp351 and a π-π stacking interaction with Trp383. It was observed that in compound **3e**, the substitution on the phenyl ring (OH) is involved in hydrogen bond, indicating the importance of the type of substitutions on the phenyl ring for the interaction of these compounds with the active site of the receptor and, consequently their cytotoxic effects. Compounds **3d** and **3g** lacked any hydrogen bonding interactions with the target enzyme, which may explain the lack of cytotoxic effects of these compounds. Furthermore, the binding free energies obtained from docking calculations supported the stability of the ligand-receptor interactions. The compounds **3e**, **3f**, and **3g** exhibited binding energies of -10.9, -10.5, and − 8.1 kcal.mol-1, respectively, compared to the co-crystallized ligand OHT (-7.7 $kcal.mol^{-1}$). These results indicate that the designed compounds have more favorable binding affinities toward ERα than the native ligand, further supporting their potential inhibitory activity.

3. Conclusion

In this study, we have developed a highly efficient and robust acid catalyst with outstanding catalytic performance. The catalyst was synthesized by integrating graphitic carbon nitride (g-C_3N_4) nanolayers—a polymeric material possessing an intrinsically porous structure and nitrogen-rich functional groups—as the support. To further enhance its catalytic versatility and activity, the g-C_3N_4 framework was functionalized with $NiFe_2O_4$ nanoparticles. The $NiFe_2O_4$ imparts both magnetic and Lewis acidic functionalities to the resulting nanocomposite, providing a multifunctional and recyclable catalytic system. Their uniform distribution over the large surface area of g-C_3N_4 facilitates improved dispersion and exposure of active sites, leading to enhanced catalytic efficiency. This purposeful modification significantly optimized the balance between acidic and basic sites of the material, resulting in a catalyst that exhibits superior efficiency and reactivity. The composite demonstrated outstanding catalytic performance in synthesizing xanthene derivatives under mild and sustainable conditions, emphasizing its potential as a highly efficient and green catalytic system for various applications. Notably, water was employed as the reaction solvent, providing a more environmentally friendly reaction medium. In addition, the cytotoxic activity of these synthesized xanthene derivatives against the MCF-7 cell line was systematically evaluated for the first time. Although the observed activities were moderate, the results provide preliminary information regarding the biological profile of these compounds and may serve as a basis for further structural optimization and biological investigations.

4. Materials and methods

All reagents and solvents were purchased from chemical companies Merck, Aldrich, and Fluka. Melting points of the synthetic materials were measured using the Buchi B-540 B. V. CHI apparatus. KBr tablets were utilized for FT-IR analysis with the Bruker Equinox 55 spectrometer. Nanoparticles size and catalyst morphology were determined using a Mira 3-XMU field emission scanning electron microscope (FE-SEM). Energy Dispersive X-ray Spectroscopy (EDX) was performed using Phenom pro X. Crystallographic properties of the sample were analyzed using an X-ray diffractometer (XRD, Philips Xpert) with Ni-filtered CuKα radiation (kCuK = 0.1542 nm), operating at 40 kV and 30 mA, within the 2θ range from 10° to 80°. Thermogravimetric analysis (TGA) was conducted using an STA 505 instrument under an argon atmosphere. The BET surface area, pore size, and pore volume were measured using a Tristar II 3020 analyzer.

4.1. Synthesis of graphitic carbon nitride (g-C_3N_4)

In order to create graphitic carbon nitride (g-C_3N_4), melamine powder (10 g) was put in a closed crucible and heated to 550°C for two hours in a muffle furnace at a regulated pace of 20°C per minute. The successful thermal polymerization of melamine was shown by the formation of a yellow powder, which is a hallmark of graphitic carbon nitride, upon natural cooling to room temperature (Scheme 1) (60).

4.2. Preparation of g-C_3N_4/$NiFe_2O_4$ nanosheets

$NiFe_2O_4$ nanoparticles were synthesized according to a previously reported procedure (61). Then, g-C_3N_4 nanosheets (1.0 g) were dispersed in ethanol (25 mL), followed by the addition of $NiFe_2O_4$ (0.5 g). The resulting mixture was ultrasonicated for 3 hours, and then stirred at room temperature for 24 hours. Finally, the obtained product was dried in an oven at 60°C (Scheme 2).

4.3. General procedure for the preparation of xanthene derivatives

β-naphthol (**1**, 2 mmol), aromatic aldehyde (**2**, 1 mmol), and g-C_3N_4/$NiFe_2O_4$ (0.04 g) as a catalyst were added to a flask containing H_2O (50 mL) and stirred at reflux temperature. Following the reaction's completion, as determined by TLC (n-Hexane/EtOAc, 3:1). After completion of the reaction, the catalyst was easily separated from the reaction mixture using an external magnet. Following the cooling of the reaction mixture to room temperature, the precipitate was filtered and given an ethanol wash. Recrystallization in ethanol was used to further purify the product (Scheme 3). The catalyst was then cleaned with hot ethanol and dried for two hours at 120°C for another use.

4.4. Cytotoxic assay

Cytotoxic activity of the synthesized compounds **(3a-3g)** was assessed using MTT assay (62). The MCF-7 cancerous cell line was obtained from the National Cell Bank of Iran (NCBI). The cancer cell line was cultured in RPMI 1640 medium supplemented with 10% fetal bovine serum (FBS) and 1% penicillin-streptomycin (Gibco, USA). Once the cells reached the desired confluence, they were harvested using a 0.5% trypsin/EDTA solution (Gibco, USA). Cells were seeded at a density of 1×10^4 cells per well in 96-well microplates and various concentrations of the synthesized derivatives and erlotinib were plated in 96-well microplates. After 48 hours, the media was aspirated, and 100 µL of a freshly prepared MTT solution was added. The plates were then incubated for an additional 4 hours at 37°C (63). Subsequently, 150 µL of DMSO was added to solubilize the formazan crystals. The absorbance of all derivatives was measured at 490 nm using a microplate ELISA reader. Data analysis was performed using Excel 2016 and Curve Expert 1.4. (64).

4.5. Molecular docking study

In order to theoretically investigate the binding pose of molecules **3a-3g** with the possible receptor, the 3D crystallography structure of the human alpha estrogen receptor, which is highly expressed in the MCF-7 cell line, with PDB code 3ERT, was retrieved from the Protein Data Bank (www.rcsb.org). Then, the original ligand (OHT) and water molecules were deleted, and Gasteiger partial charges were added to the receptor. The structures of the target ligands were drawn, optimized for geometry, and minimized for energy, then saved in PDBQT format using ChemDraw, Chem3D, and AutoDock Tools. The grid box was set to a size of 40×40×40 Å, with its center positioned at the coordinates of the native ligand (X = 30.282, Y=-1.1913, Z = 24.207). The analysis of interactions between ligands **3a**-**3g** and the active site of the receptor was carried out using Discovery Studio 2016.

Abbreviations

FT-IR
Fourier Transform Infrared
FE-SEM
Field Emission Scanning Electron Microscope
NMR
Nuclear Magnetic Resonance
TLC
Thin Layer Chromatography
EtOH
Ethanol
MCRs
Multi-Component Reactions
S-F
solvent free
g-C_3N_4
Graphitic carbon nitride.

Declarations

Acknowledgments

Financial assistance from Shiraz University of Medical Sciences, as indicated by grant number 31240, is gratefully acknowledged.

Availability of data and materials

The datasets generated or analyzed during this research are accessible from the corresponding author upon reasonable request.

Declarations

Ethics approval and consent to participate

Not applicable.

Consent for publication

Not applicable.

Competing interests

The authors declare no competing interests.

Authors' contributions

L.AZ. designed and performed the research; A.ST. analyzed the data; S.S. achieved Molecular docking study and Cytotoxicity study; Z.K. made the assay and conducted the optimization; SH.N. Review and editing; S.Kh. interpreted the results and prepared the manuscript. All authors read and approved the final manuscript.

References

1. Shen, X., Hong, G. & Wang, L. Recent advances in green multi-component reactions for heterocyclic compound construction. *Org. Biomol. Chem.* **23** (9), 2059–2078 (2025).
2. Lefebvre, M., Johnson, P. A. & Deslongchamps, P. The Mechanism of the Cycloaddition of Substituted Ketenes to Cyclopentadiene Based on the Bent Bond/Antiperiplanar Hypothesis Orbital Model. *J. Org. Chem.* **90** (8), 2831–2841 (2025).
3. Aricò, F. *Green synthesis of heterocycles* p. 74 (Frontiers Media SA, 2020).
4. Khabnadideh, S., Mirzaei, E. & Amiri-Zirtol, L. L-arginine modified graphene oxide: A novel heterogeneous catalyst for synthesis of benzo [b] pyrans and pyrano [3, 2–c] chromenes. *J. Mol. Struct.* **1261**, 132934 (2022).
5. Tonjes, D. J. & Mallikarjun, S. Cost effectiveness of recycling: A systems model. *Waste Manage.* **33** (11), 2548–2556 (2013).
6. Shende, V. S., Saptal, V. B. & Bhanage, B. M. Recent advances utilized in the recycling of homogeneous catalysis. *Chem. Record*. **19** (9), 2022–2043 (2019).
7. Hara, M., Nakajima, K. & Kamata, K. Recent progress in the development of solid catalysts for biomass conversion into high value-added chemicals. *Sci. Technol. Adv. Mater.* **16** (3), 034903 (2015).
8. Khabnadideh, S. et al. Efficient synthesis of 1, 3-naphtoxazine derivatives using reusable magnetic catalyst (GO-Fe3O4–Ti (IV)): anticonvulsant evaluation and computational studies. *BMC Chem.* **16** (1), 44 (2022).
9. Amiri-Zirtol, L., Amrollahi, M. A. & Mirjalili, B-F. GO-Fe3O4-Ti (IV) as an efficient magnetic catalyst for the synthesis of bis (indolyl) methanes and benzo [a] xanthen-11-one derivatives. *Inorg. Nano-Metal Chem.* **53** (11), 1211–1221 (2023).
10. Amiri-zirtol, L. et al. A novel and efficient boron-containing magnetic catalyst based on graphene oxide (GO-Fe3O4-BFn) for synthesis of pyrazole and pyranopyrazole derivatives. *J. Mol. Struct.* **1307**, 137868 (2024).
11. Singh, K. K. International Journal of New Chemistry. *Int. J. New. Chem.* **9** (3), 361–372 (2022).
12. Liu, M. et al. Recent advances of magnetite (Fe3O4)-based magnetic materials in catalytic applications. *Magnetochemistry* **9** (4), 110 (2023).

13. Cotty, S. et al. Electrochemical recycling of homogeneous catalysts. *Sci. Adv.* **8** (42), eade3094 (2022).
14. Liu, Y. et al. NiFe2O4/g-C3N4 heterojunction composite with enhanced visible-light photocatalytic activity. *J. Saudi Chem. Soc.* **22** (4), 439–448 (2018).
15. Abbas, N. & Kim, T. H. Cubic Cu_2O-Decorated B-doped g-C_3N_4 nanosheets for ultrasensitive electrochemical detection of Metol. *J. Environ. Chem. Eng.* :118489. (2025).
16. Xing, R. et al. Novel solid acid catalysts: sulfonic acid group-functionalized mesostructured polymers. *Adv. Funct. Mater.* **17** (14), 2455–2461 (2007).
17. Amiri-Zirtol, L. & Gholami, A. Innovative synthesis of nano-magnetic bio-organocatalysts from red mud waste for green polyhydroquinoline derivatives synthesis. *Sci. Rep.* **14** (1), 26143 (2024).
18. Bosica, G., Baldacchino, K., Abdilla, R. & De Nittis, R. Green organic synthesis via multicomponent reactions. (2021).
19. Graziano, G. et al. Multicomponent reaction-assisted drug discovery: a time-and cost-effective green approach speeding up identification and optimization of anticancer drugs. *Int. J. Mol. Sci.* **24** (7), 6581 (2023).
20. Mohlala, R. L., Rashamuse, T. J. & Coyanis, E. M. Highlighting multicomponent reactions as an efficient and facile alternative route in the chemical synthesis of organic-based molecules: a tremendous growth in the past 5 years. *Front. Chem.* **12**, 1469677 (2024).
21. Khabnadideh, S., Khorshidi, K. & Amiri-Zirtol, L. A novel heterogeneous acid–base nano-catalyst designed based on graphene oxide for synthesis of spiro-indoline-pyranochromene derivatives. *BMC Chem.* **17** (1), 12 (2023).
22. Ghahsare, A. G., Nazifi, Z. S. & Nazifi, S. M. Structure-bioactivity relationship study of xanthene derivatives: a brief review. *Curr. Org. Synth.* **16** (8), 1071–1077 (2019).
23. Bader, M. et al. *Xanthine derivatives, their use as a medicament, and pharmaceutical preparations comprising the same* (Google Patents, 2020).
24. Lazić, A. M., Mašulović, A. D., Lađarević, J. M. & Valentić, N. V. Assessing the pharmacological potential of selected xanthene derivatives. *J. Serb. Chem. Soc.* **88** (9), 811–824 (2023).
25. Burange, A. S. et al. Green synthesis of xanthene and acridine-based heterocycles of pharmaceutical importance: a review. *Environ. Chem. Lett.* **19** (4), 3283–3314 (2021).
26. Moradi, L. & Mirzaei, M. Immobilization of Lewis acidic ionic liquid on perlite nanoparticle surfaces as a highly efficient solid acid catalyst for the solvent-free synthesis of xanthene derivatives. *RSC Adv.* **9** (35), 19940–19948 (2019).
27. Singh, H., Kumari, S. & Khurana, J. M. A new green approach for the synthesis of 12-aryl-8, 9, 10, 12-tetrahydrobenzo [a] xanthene-11-one derivatives using task specific acidic ionic liquid [NMP] H2PO4. *Chin. Chem. Lett.* **25** (10), 1336–1340 (2014).
28. Bosica, G., De Nittis, R. & Borg, R. Solvent-free, one-pot, multicomponent synthesis of xanthene derivatives. *Catalysts* **13** (3), 561 (2023).

29. Khosropour, A. R., Khodaei, M. M. & Moghannian, H. A facile, simple and convenient method for the synthesis of 14-alkyl or aryl-14-H-dibenzo [a, j] xanthenes catalyzed by pTSA in solution and solvent-free conditions. *Synlett* **2005** (06), 0955–0958 (2005).
30. Eshghi, H. & Mirzaie, N. Ferric hydrogensulphate as a recyclable catalyst for the synthesis of fluorescein derivatives. *Chem. Pap.* **65** (4), 504–509 (2011).
31. Akbari, A. One-pot synthesis of dihydropyrano [c] chromene derivatives by using BF3• SiO2 as catalyst. *Heterocycl. Commun.* **19** (6), 425–427 (2013).
32. Atkore, S. T. et al. Synthesis of 14-substituted-14H-Dibenzo [a, j] xanthene derivatives in presence of effective synergetic catalytic system bleaching earth clay and PEG-600. *Catalysts* **11** (11), 1294 (2021).
33. Salama, R. S., El-Bahy, S. M. & Mannaa, M. A. Sulfamic acid supported on mesoporous MCM-41 as a novel, efficient and reusable heterogenous solid acid catalyst for synthesis of xanthene, dihydropyrimidinone and coumarin derivatives. *Colloids Surf., A*. **628**, 127261 (2021).
34. Mohamadpour, F., Maghsoodlou, M. T., Lashkari, M., Heydari, R. & Hazeri, N. Green synthesis of polysubstituted quinolines and xanthene derivatives promoted by tartaric acid as a naturally green catalyst under solvent-free conditions. *Chem. J. Moldova*. **13** (1), 74–86 (2018).
35. Chaudhary, A. & Khurana, J. M. Advances in the synthesis of xanthenes: an overview. *Curr. Org. Synth.* **15** (3), 341–369 (2018).
36. Devi, C. U. et al. Hetero-structured NiFe2O4/g-C3N4 as dual-functional catalyst for the maximized photocatalytic degradation and electrochemical HER performance. *J. Mater. Sci.: Mater. Electron.* **36** (33), 2128 (2025).
37. Palanivel, B., Siva, G., Hossain, M. S. & Shkir, M. Facile design of N-rich g-C_3N_5/NiFe2O4 heterojunction for visible-light-driven photo-Fenton RhB degradation and photocatalytic hydrogen evolution. *Diam. Relat. Mater.* :112801. (2025).
38. Maleki, B. & Esmaeili, H. Upgrading of NiFe2O4 via decoration of g-C3N4 nanoparticles to a magnetic catalyst for the ultrasound-assisted production of biodiesel. *Sci. Rep.* (2025).
39. Nguyen, L. T. T. et al. Synthesis of magnetic NiFe2O4/g-C3N4 heterojunction photocatalysts for boosting dye degradation performance under visible-light irradiation. *Nanoscale Adv.* **7** (2), 536–548 (2025).
40. Ruotolo, L. M., Silva, R. R. & Nogueira, F. G. E. Peroxymonosulfate Activation by Magnetic Nife2o4/G-C3n4 for Tetracycline Hydrochloride Degradation Under Visible Light. Available at SSRN 4524371.
41. Ahmed, A. et al. Advances in inorganic NiFe2O4/g-C3N4 composite catalysts: Synthesis, characterization, and application in peroxymonosulfate activation for antibiotic degradation. *Inorg. Chem. Commun.* :115581. (2025).
42. Wang, J. & Wang, S. A critical review on graphitic carbon nitride (g-C3N4)-based materials: Preparation, modification and environmental application. *Coord. Chem. Rev.* **453**, 214338 (2022).
43. Liu, S., Zada, A., Yu, X., Liu, F. & Jin, G. NiFe2O4/g-C3N4 heterostructure with an enhanced ability for photocatalytic degradation of tetracycline hydrochloride and antibacterial performance.

Chemosphere **307**, 135717 (2022).

44. Elamin, M. R. et al. Efficient NiFe2O4@ g-C3N4 nanosorbent for oxytetracycline adsorption: removal modeling and selectivity. *J. Electron. Mater.* **53** (10), 6164–6180 (2024).
45. Nguyen, L. T. T. et al. Synthesis of magnetic NiFe 2 O 4/gC 3 N 4 heterojunction photocatalysts for boosting dye degradation performance under visible-light irradiation. *Nanoscale Adv.* **7** (2), 536–548 (2025).
46. https://www.icdd.com/ Af.
47. Ji, H. et al. Magnetic gC 3 N 4/NiFe 2 O 4 hybrids with enhanced photocatalytic activity. *RSC Adv.* **5** (71), 57960–57967 (2015).
48. Mishra, S., Acharya, L., Sharmila, S., Sanjay, K. & Acharya, R. Designing g-C3N4/NiFe2O4 S-scheme heterojunctions for efficient photocatalytic degradation of Rhodamine B and tetracycline hydrochloride. *Appl. Surf. Sci. Adv.* **24**, 100647 (2024).
49. Behbahani, F. K. & Valiallahi, M. Synthesis of 14-aryl-14H-dibenzo [a, j] xanthenes using CuSO4· 5H2O as a green and reusable catalyst. *Arab. J. Chem.* **10**, S1686–S9 (2017).
50. Ziarani, G. M., Badiei, A-R. & Azizi, M. The one-pot synthesis of 14-aryl-14H-dibenzo [a, j] xanthene derivatives using sulfonic acid functionalized silica (SiO2-Pr-SO3H) under solvent free conditions. *Scientia Iranica*. **18** (3), 453–457 (2011).
51. Hojati, S. F., Moosavifar, M. & Moeinieghbali, N. One-pot three-component synthesis of 1, 8-dioxooctahydroxanthenes and 14-Aryl-14Hdibenzo [a, j] xanthenes using a new nanostructure zeolite. *J. Chem. Sci.* **132** (1), 38 (2020).
52. Metwally, H. M. et al. Natural oils as emulsifying agent in the eco-friendly preparation of nano ZnO and their catalytic evaluation in the synthesis of 1, 8-dioxo-octahydroxanthene derivatives with anti-inflammatory activity: In vitro, docking validation, and dft calculations. *Bull. Chem. Soc. Ethiop.* **39** (9), 1779–1793 (2025).
53. Alipour, A., Naeimi, H., Alipour, H. & Naeimi Design, fabrication and characterization of magnetic nickel copper ferrite nanocomposites and their application as a reusable nanocatalyst for sonochemical synthesis of 14-aryl-14-H-dibenzo [a, j] xanthene derivatives: A. *Res. Chem. Intermed.* ;**49**(6):2705–2723. (2023).
54. Farsi, R. & Saghanezhad, S. J. Green synthesis of 14-aryl-14H-dibenzo [a, j] xanthene derivatives using sulfonic acid-supported magnetic covalent organic framework as a novel and reusable nanostructured catalyst. *Res. Chem. Intermed.* **50** (9), 4229–4247 (2024).
55. Kumar, A., Rout, L., Achary, L. S. K., Dhaka, R. S. & Dash, P. Greener route for synthesis of aryl and alkyl-14H-dibenzo [aj] xanthenes using graphene oxide-copper ferrite nanocomposite as a recyclable heterogeneous catalyst. *Sci. Rep.* **7** (1), 42975 (2017).
56. Kiasat, R. A., Mouradzadegun, A. & Saghanezhad, J. S. Phosphosulfonic acid, an efficient solid acid catalyst for the one-pot preparation of 14-aryl-14H-dibenzo [a, j] xanthenes and 1, 8-dioxo-octahydro-xanthenes under solvent-free conditions. *J. Serb. Chem. Soc.* **78** (9), 1291–1299 (2013).

57. Saghanezhad, S. J., Nazari, Y. & Davod, F. Cucurbit [6] uril-OSO 3 H: a novel acidic nanocatalyst for the one-pot preparation of 14-aryl-14 H-dibenzo [a, j] xanthenes and 1, 8-dioxo-octahydro-xanthenes. *RSC Adv.* **6** (30), 25525–25530 (2016).
58. Tan, H., Zhong, Y. & Pan, Z. Autocrine regulation of cell proliferation by estrogen receptor-alpha in estrogen receptor-alpha-positive breast cancer cell lines. *BMC cancer*. **9** (1), 31 (2009).
59. Zivadinovic, D., Gametchu, B. & Watson, C. S. Membrane estrogen receptor-α levels in MCF-7 breast cancer cells predict cAMP and proliferation responses. *Breast Cancer Res.* **7** (1), R101 (2004).
60. Tonda, S., Kumar, S., Gawli, Y., Bhardwaj, M. & Ogale, S. g-C3N4 (2D)/CdS (1D)/rGO (2D) dual-interface nano-composite for excellent and stable visible light photocatalytic hydrogen generation. *Int. J. Hydrog. Energy*. **42** (9), 5971–5984 (2017).
61. Kavas, H., Kasapoğlu, N., Baykal, A. & Köseoğlu, Y. Characterization of NiFe2O4 nanoparticles synthesized by various methods. *Chem. Pap.* **63** (4), 450–455 (2009).
62. Baziar, L. et al. Design, synthesis, biological evaluation and computational studies of 4-Aminopiperidine-3, 4-dihyroquinazoline-2-uracil derivatives as promising antidiabetic agents. *Sci. Rep.* **14** (1), 26538 (2024).
63. Emami, L. et al. 6-Bromo quinazoline derivatives as cytotoxic agents: design, synthesis, molecular docking and MD simulation. *BMC Chem.* **18** (1), 125 (2024).
64. Emami, M. et al. Multifunctional Bi-layer collagen nanofiber-collagen/PLLA/Zataria multiflora essential oil nanofiber for wound healing: Antibacterial, antifungal and antioxidant properties. *J. Drug Deliv. Sci. Technol.* **92**, 105285 (2024).

Scheme

Scheme figures 1-3 are available in the Supplementary Files section.

Figures

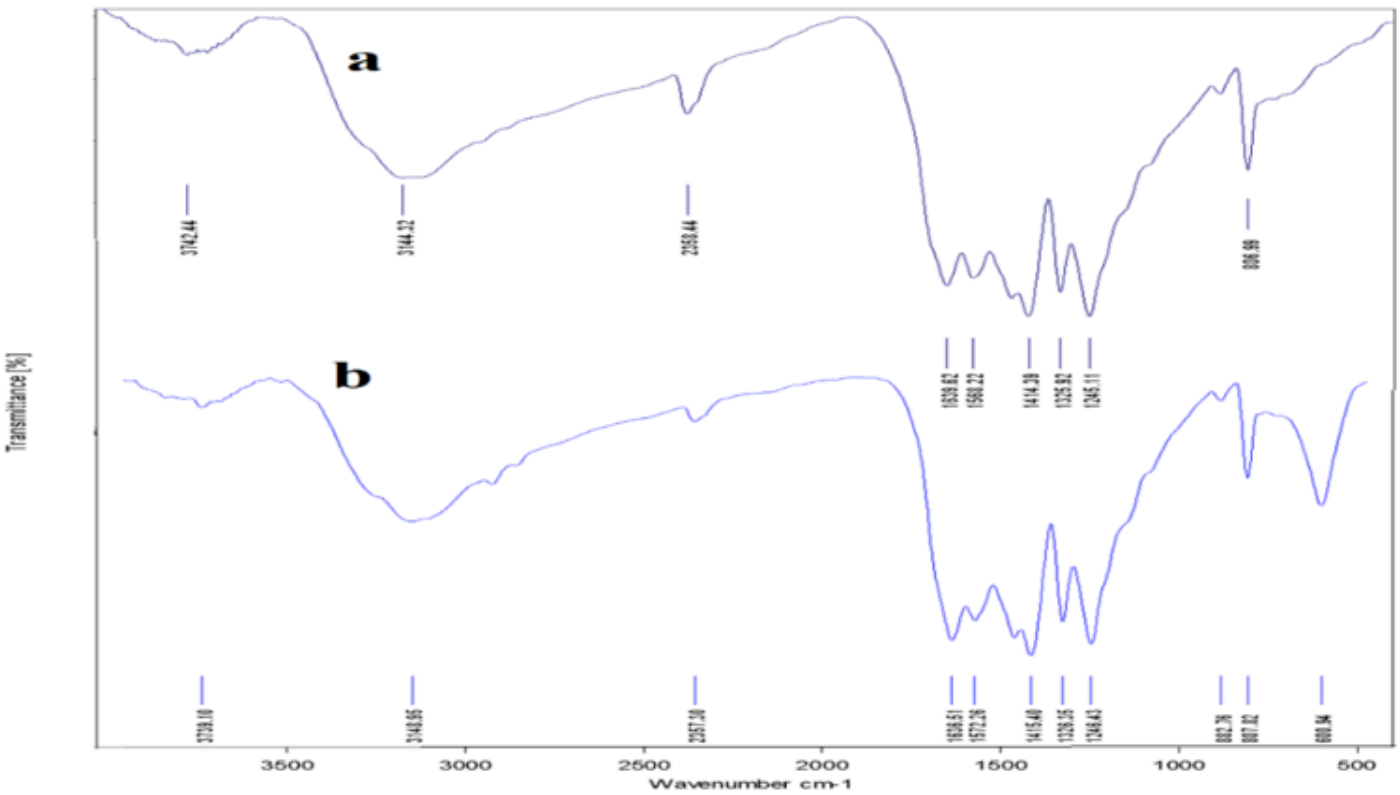


Figure 1

FT-IR spectrum of g-C_3N_4 (a), and nano- g-C_3N_4/$NiFe_2O_4$ (b)

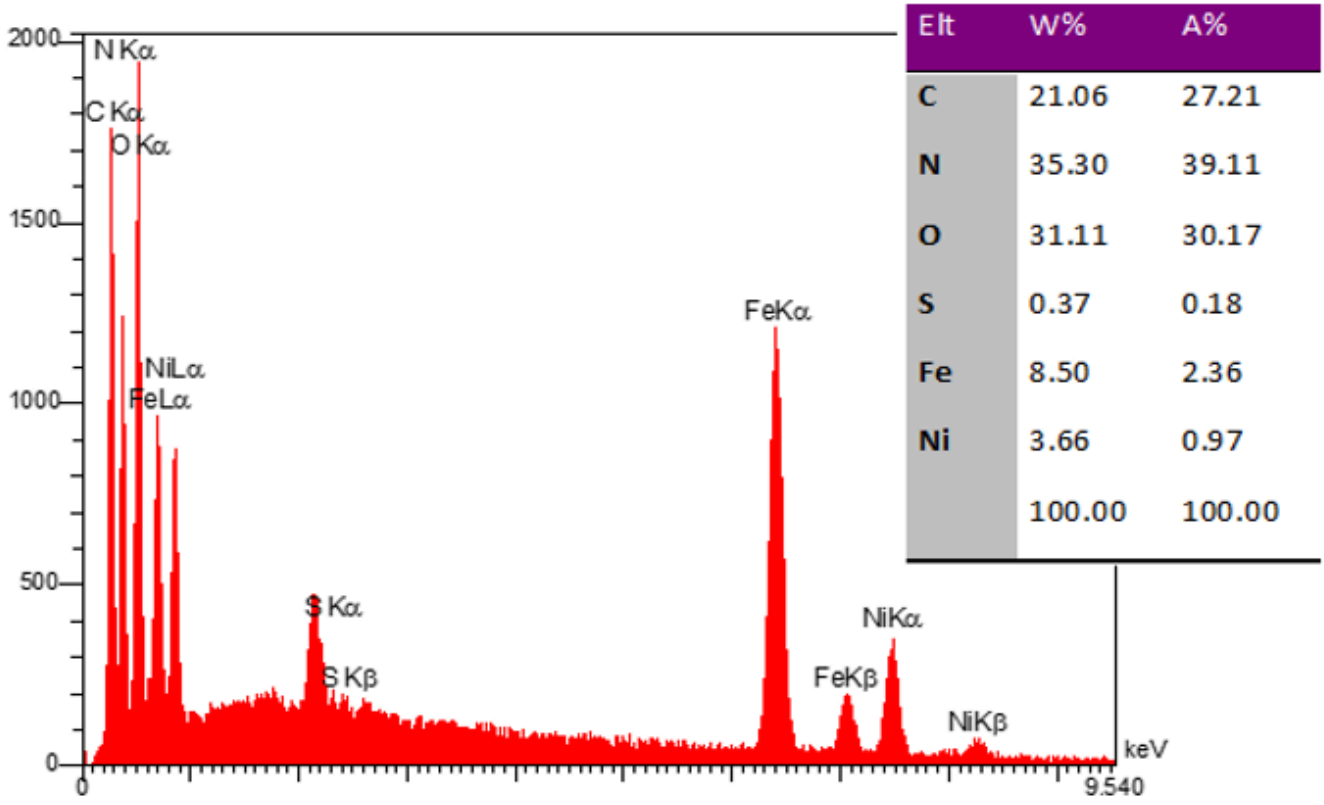


Figure 2

EDX spectrum of nano- g-C_3N_4/$NiFe_2O_4$

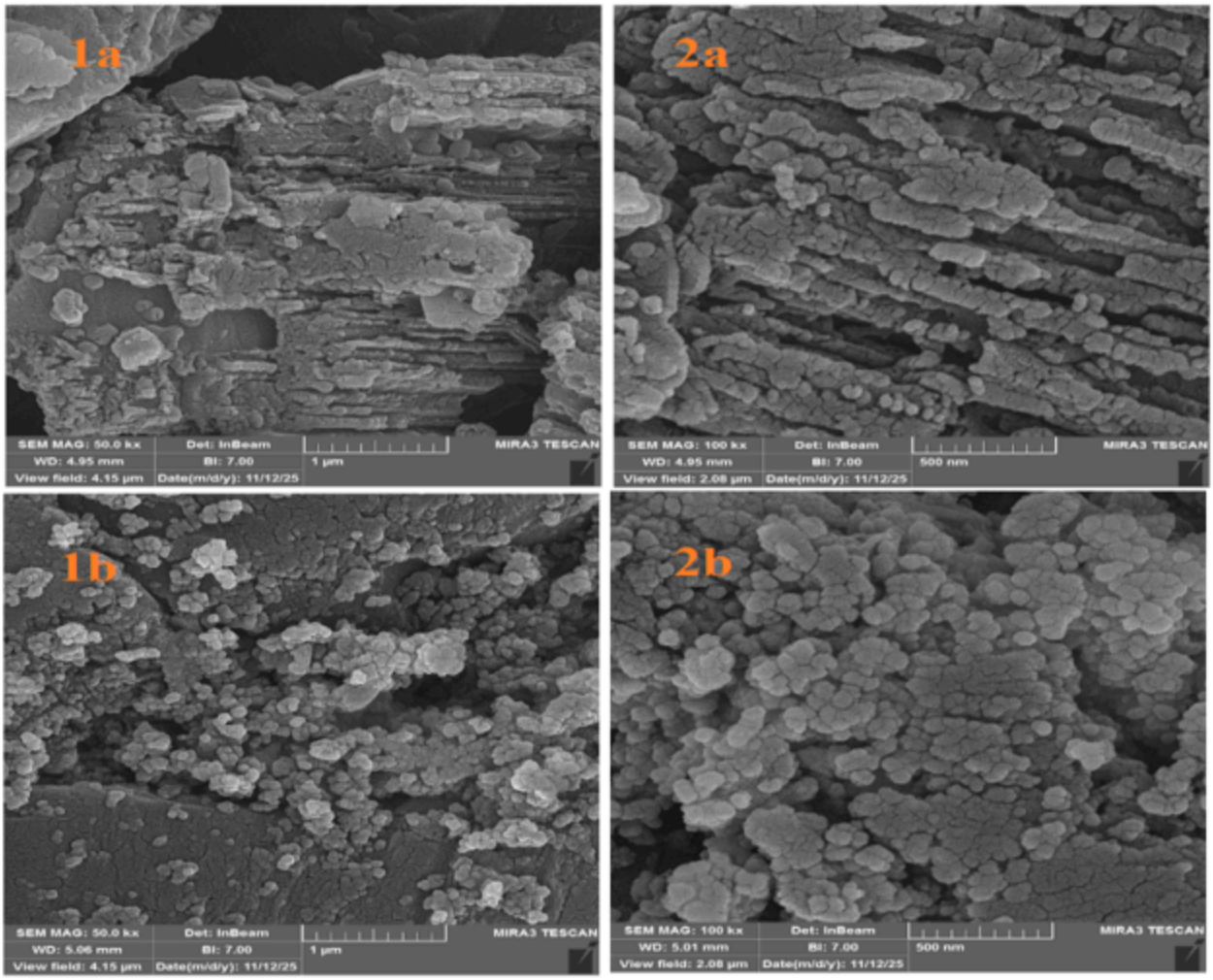


Figure 3

SEM spectrum of nano- g-C_3N_4 (1a and 2a), and nano- g-C_3N_4/$NiFe_2O_4$ (1b and 2b)

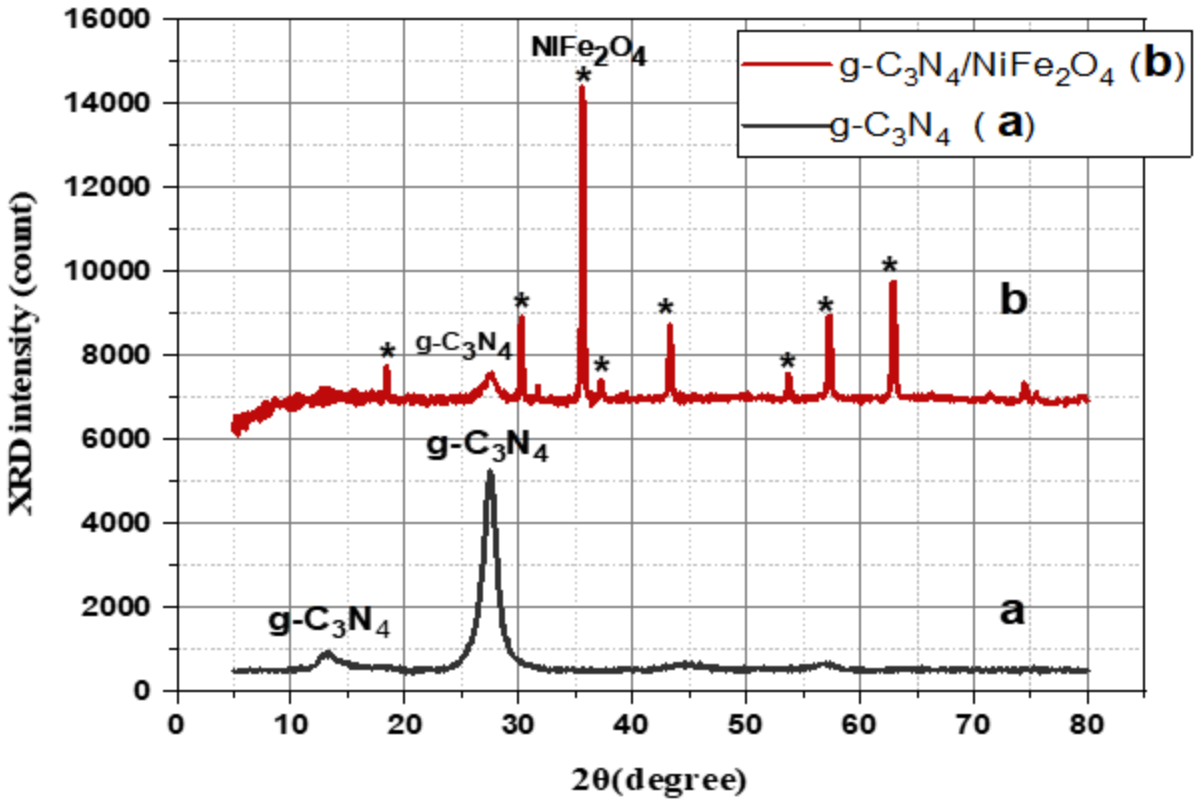


Figure 4

XRD patterns of g-C_3N_4 (a), and g-C_3N_4/$NiFe_2O_4$ (b)

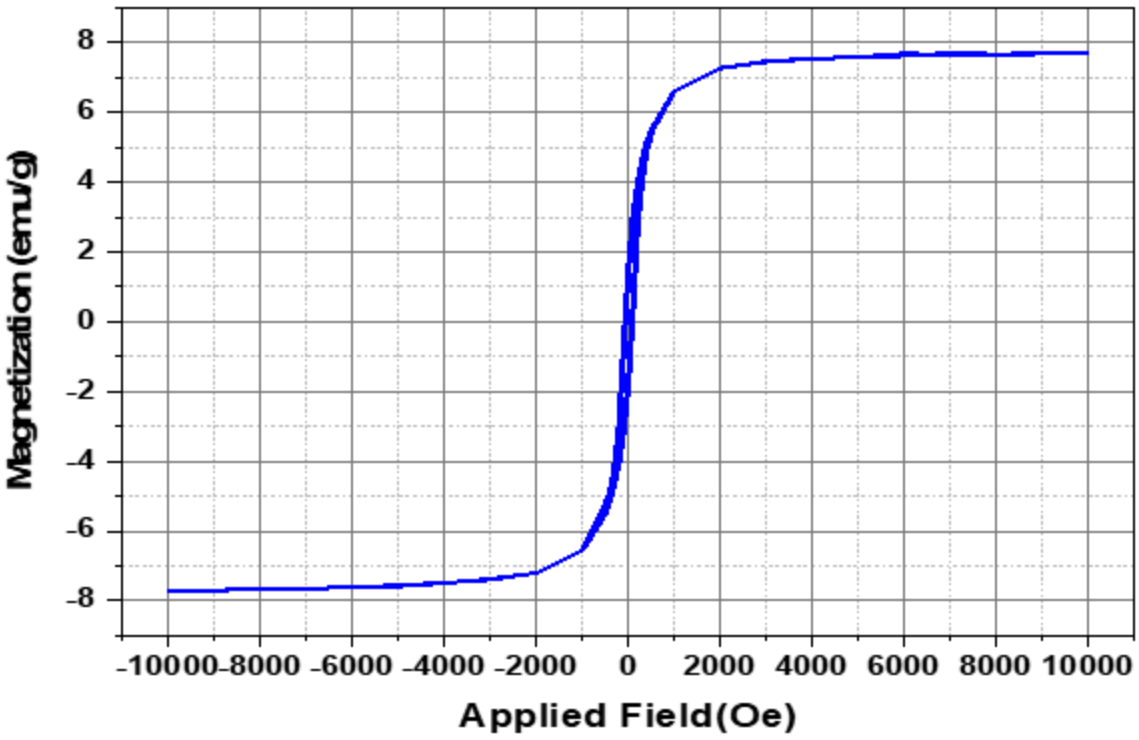


Figure 5

VSM magnetic analysis of g-C_3N_4/$NiFe_2O_4$

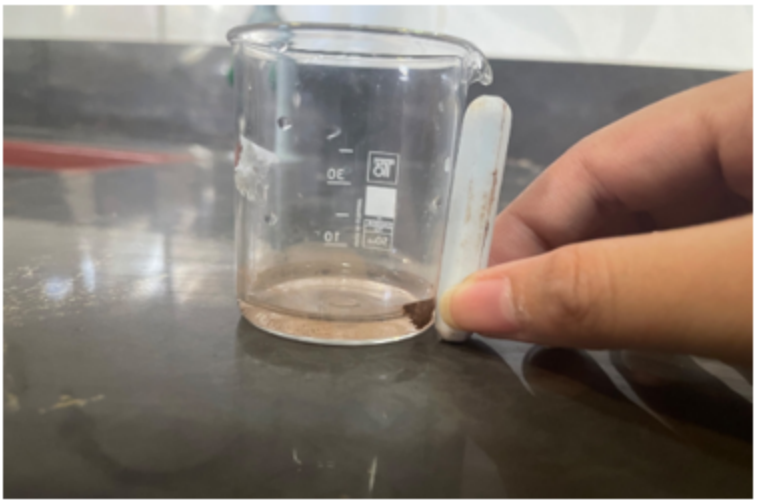


Figure 6

The magnetic behavior of g-C_3N_4/$NiFe_2O_4$

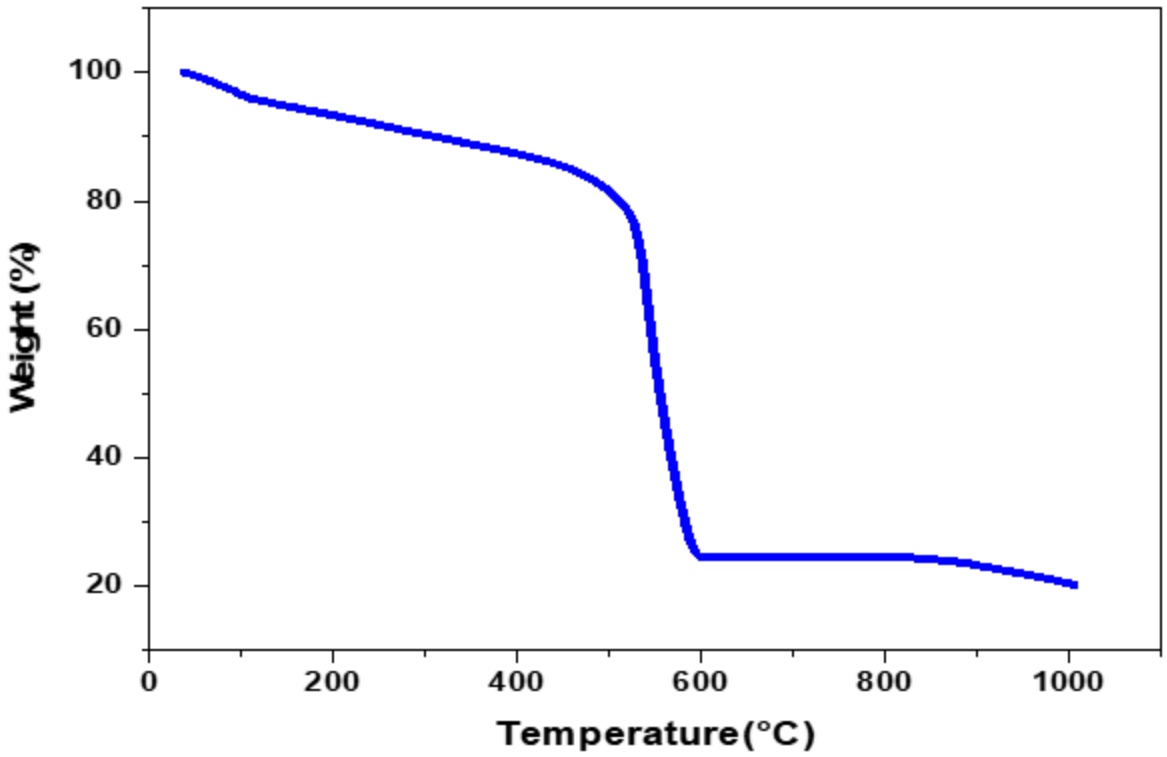


Figure 7

TGA analysis of g-C_3N_4/$NiFe_2O_4$

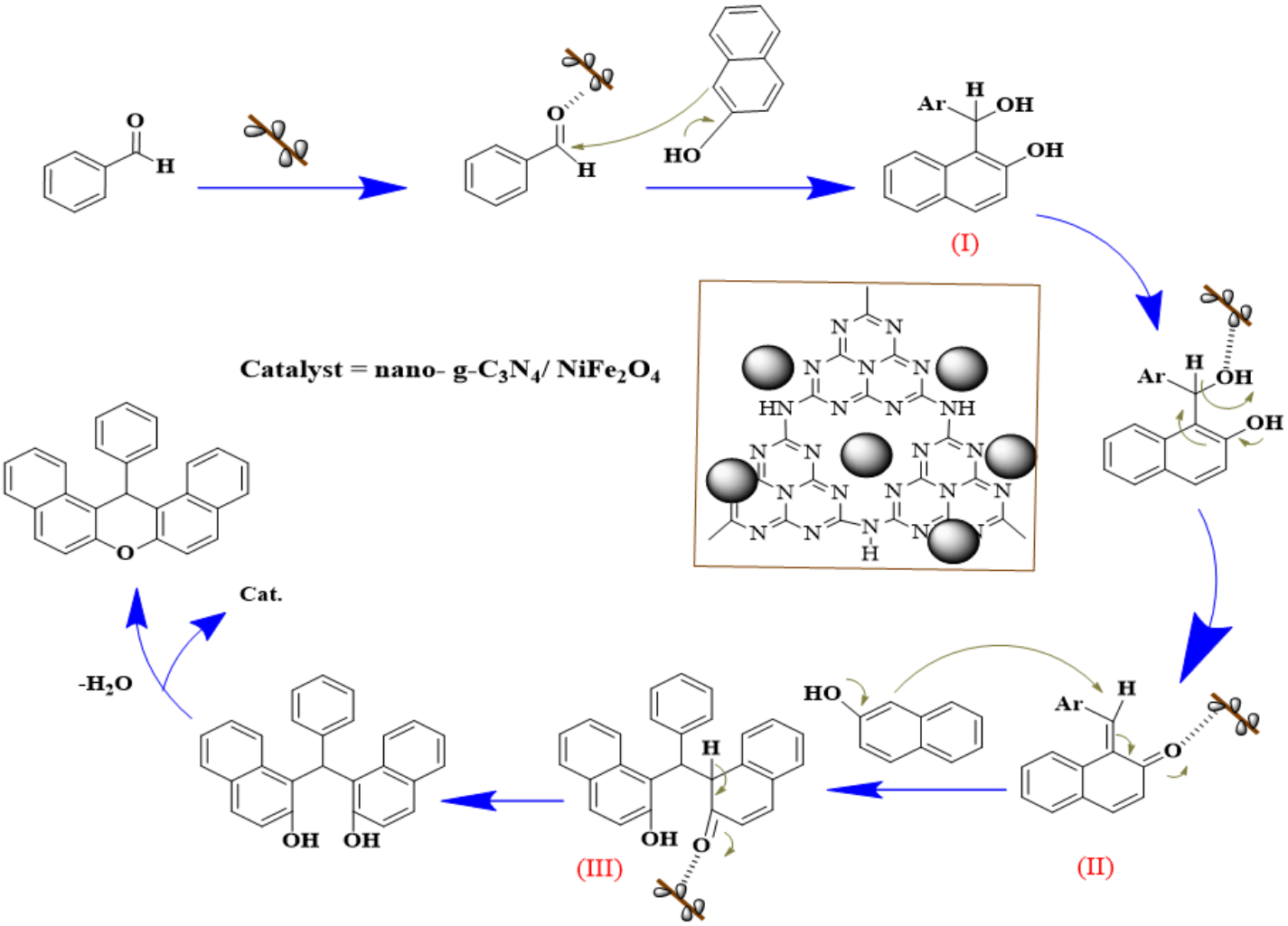


Figure 8

The proposed mechanism for synthesis of xanthene derivatives catalyzed by g-C_3N_4/$NiFe_2O_4$

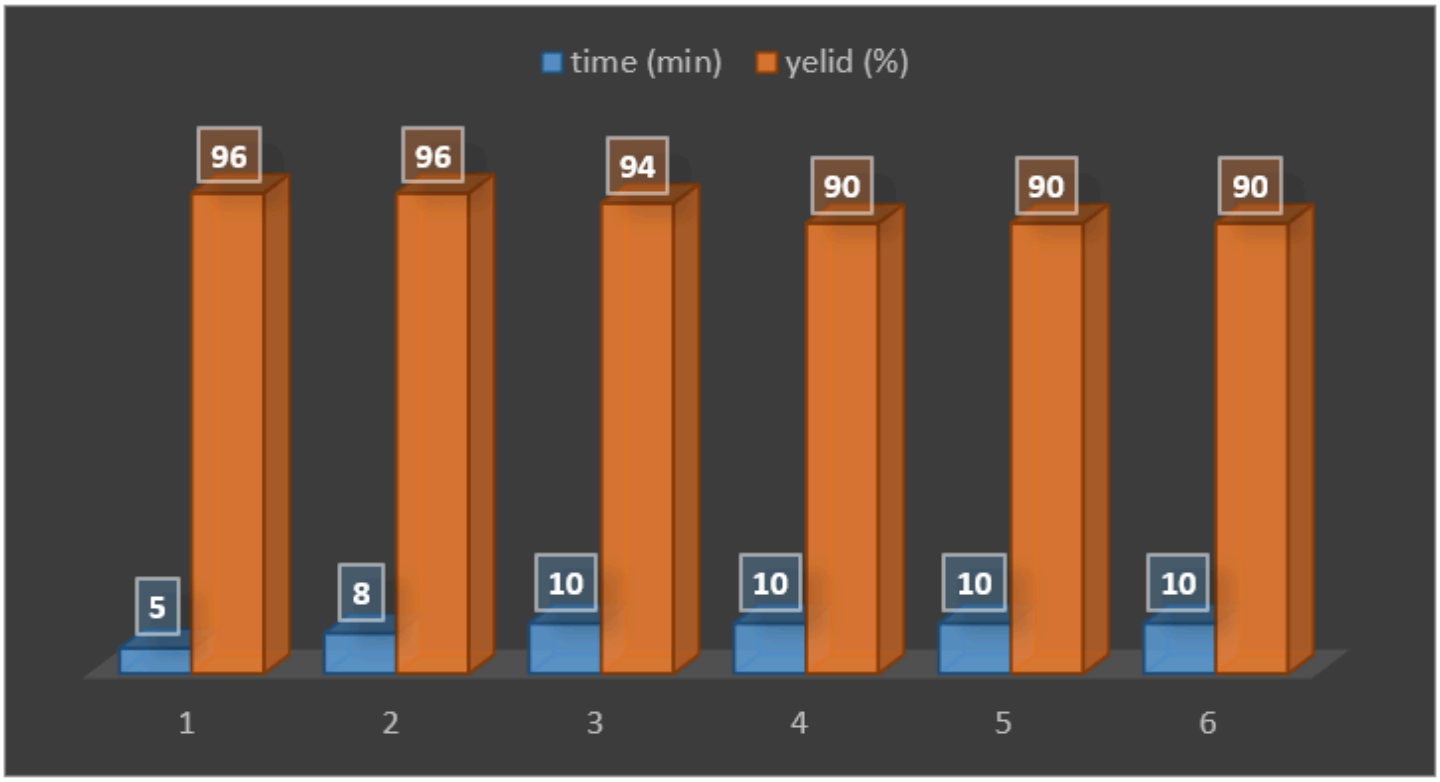


Figure 9

Recyclability of catalyst g-C_3N_4/$NiFe_2O_4$

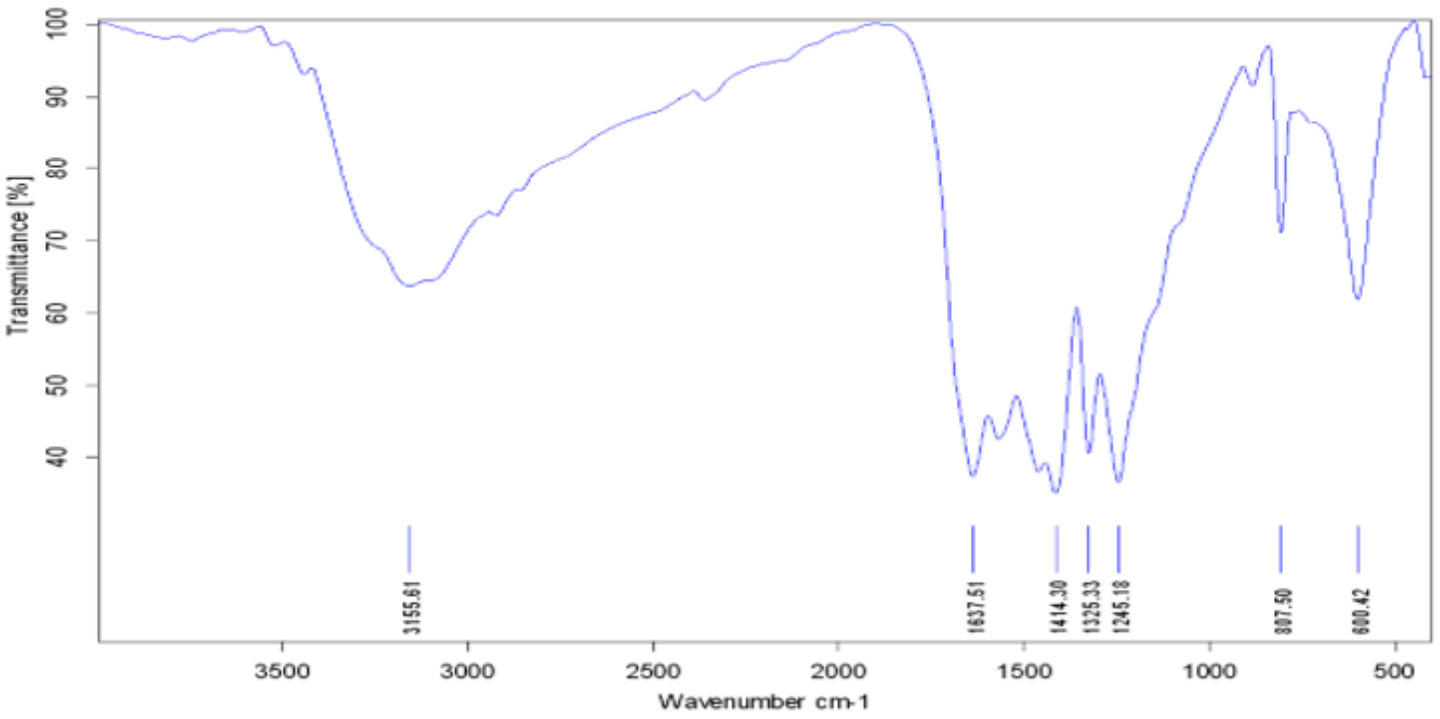


Figure 10

FT-IR of the used nano g-C_3N_4/$NiFe_2O_4$

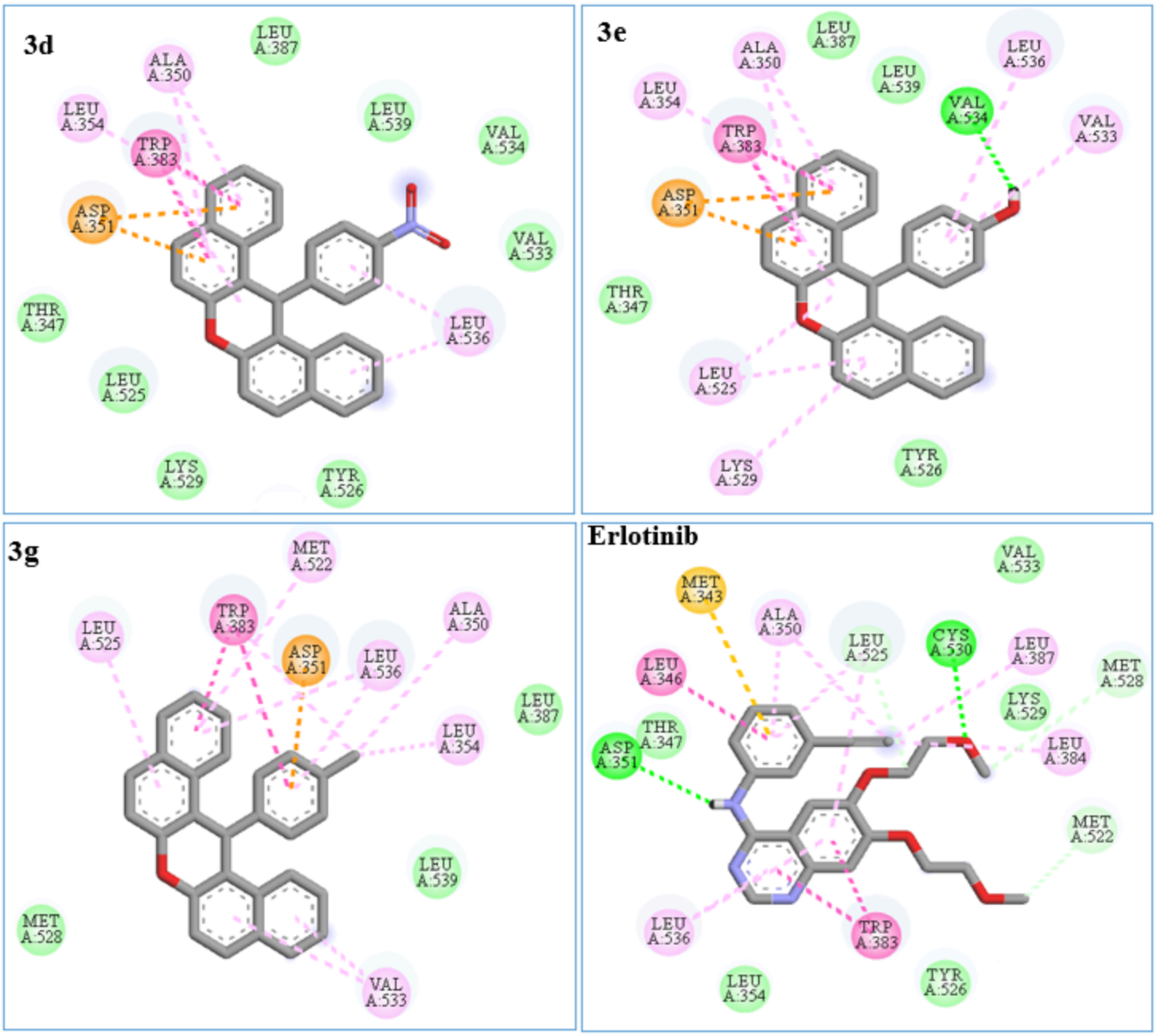


Figure 11

The interaction of the compounds **3d**, **3e**, **3g**, and erlotinib in the active site of ERα (3ERT). (green: Vander waals, light green: carbon hydrogen bond, dark green: hydrogen bond, dark pink: π-π, light pink: alkyl & π-alkyl, purple: π-sigma, orange: π-sulfur)

Supplementary Files

This is a list of supplementary files associated with this preprint. Click to download.

- Tables.docx
- Supplementarymaterials.docx
- Scheme1.png
- Scheme2.png
- Scheme3.png